Bolgiano-Obukhov spectrum and mixing efficiency in stably stratified turbulence

Shadab Alam [1,*] Mahendra K. Verma [2,†] and Pranav Joshi [1,‡]
[1]*Department of Mechanical Engineering, Indian Institute of Technology Kanpur, Kanpur 208016, India*
[2]*Department of Physics, Indian Institute of Technology Kanpur, Kanpur 208016, India*

(Received 29 November 2022; accepted 24 April 2023; published 17 May 2023)

In this paper, using a shell model, we simulate highly turbulent stably stratified flow for weak to moderate stratification at unitary Prandtl number. We investigate the energy spectra and fluxes of velocity and density fields. We observe that for moderate stratification, in the inertial range, the kinetic energy spectrum $E_u(k)$ and the potential energy spectrum $E_b(k)$ show dual scaling—Bolgiano-Obukhov scaling [$E_u(k) \sim k^{-11/5}$ and $E_b(k) \sim k^{-7/5}$] for $k < k_B$, where k_B is the Bolgiano wave number, and Kolmogorov scaling ($\sim k^{-5/3}$) for $k > k_B$. In addition, we find that the mixing efficiency $\eta_{\rm mix}$ varies as $\eta_{\rm mix} \sim {\rm Ri}$ for weak stratification, whereas $\eta_{\rm mix} \sim {\rm Ri}^{1/3}$ for moderate stratification, where Ri is the Richardson number.

DOI: 10.1103/PhysRevE.107.055106

I. INTRODUCTION

Stably stratified turbulence (SST) is a common phenomenon in geophysical and astrophysical fluid flows [1–6]. The presence of stabilizing density gradients in these flows, primarily due to the ubiquity of the vertical temperature gradients in the atmosphere and the vertical salinity and temperature gradients in the oceans [7,8], plays a vital role in controlling the vertical transfer of heat and the concentrations of a pollutant [9–12]. Thus, it is essential to understand the dynamics of stably stratified flows. Some of the recent review papers which detail several important features of stratified flows are by Riley and Lelong [13], Gregg *et al.* [14], and Caulfield [15].

Stably stratified turbulent flows are classified into three different regimes [2,16]—(i) weakly SST (Ri $\ll 1$ and Re $\gg 1$), (ii) moderately SST (Ri ≈ 1 and Re $\gg 1$), and (iii) strongly SST (Ri $\gg 1$ and Re $\gg 1$), where Ri and Re are the Richardson number and Reynolds number, respectively, and are defined as follows [17]:

$$\mathrm{Ri} = \frac{\mathrm{g}\rho'_{\rm rms}L}{\rho_m U^2}, \quad \mathrm{Re} = \frac{UL}{\nu},$$

where $\rho'_{\rm rms}$ is the root mean square (rms) of the density fluctuations and ρ_m is the mean density, U is the rms velocity, L is the integral length scale, g is the acceleration due to gravity, and ν is kinematic viscosity. It is customary to define the density fluctuations ρ' in the dimensions of velocity by employing the following transformation [1,2,18,19]:

$$b = \frac{\mathrm{g}}{N}\frac{\rho'}{\rho_m},$$

where b is the density fluctuation in velocity units and N is the Brunt-Väisälä frequency (defined in Sec. II). We express Ri in terms of b and N as follows:

$$\mathrm{Ri} = \frac{Nb_{\rm rms}L}{U^2}.$$

Stratification strength is also quantified by the Froude number ${\rm Fr} = U/(NL)$. The Froude number and the Richardson number are closely connected: ${\rm Ri} \approx {\rm Fr}^{-2}$ (Rosenberg *et al.* [18], Verma [2]). Another important parameter which provides a relative measure of inertial and viscous forces in stratified flows is the buoyancy Reynolds number Re_b [1,20–22],

$$\mathrm{Re}_b = \frac{\epsilon_u}{\nu N^2},$$

where $\epsilon_u = 2\nu\langle S_{ij}S_{ij}\rangle$ is the kinetic energy dissipation rate and S_{ij} is the strain rate tensor. Note that the three parameters Re_b, Re, and Fr are not independent since $\mathrm{Re}_b \approx \mathrm{ReFr}^2$ [1,22].

Bolgiano [17] and Obukhov [23] formulated a phenomenology for moderately SST, which is commonly known as the Bolgiano-Obukhov (BO) phenomenology. The BO phenomenology assumes that a substantial amount of the supplied kinetic energy is transformed into potential energy by generating density fluctuations, which then ultimately diffuse through molecular effects, i.e., $\epsilon_b \approx \epsilon_{\rm inj}$, where $\epsilon_{\rm inj}$ is the kinetic energy injection rate and $\epsilon_b = \kappa\langle|\nabla b|^2\rangle$ is the potential energy dissipation rate; κ is density diffusivity. Only a small portion of the injected kinetic energy is dissipated through viscous dissipation, i.e., $\epsilon_u \ll \epsilon_{\rm inj}$. In addition, the BO phenomenology assumes that the potential energy flux $\Pi_b(k) \approx$ const in the inertial range, and it equals the dissipation rate of the potential energy, i.e., $\Pi_b(k) = \epsilon_b$. Using these assumptions and balancing the buoyancy and nonlinear terms in the momentum equation (since Ri ≈ 1), Bolgiano [17] and Obukhov [23] predicted that the kinetic energy (KE) spectrum $E_u(k)$ and the potential energy (PE) spectrum $E_b(k)$, respectively, exhibit $k^{-11/5}$ and $k^{-7/5}$ scalings for small wave numbers ($k_L < k \leqslant k_B$), where k_B and $k_L \approx 2\pi/L$ are the Bolgiano

*Corresponding author: shadab@iitk.ac.in
†mkv@iitk.ac.in
‡jpranavr@iitk.ac.in

and integral-scale wave numbers, respectively. These scalings are collectively known as BO scaling. For $k > k_B$, buoyancy weakens and both the spectra follow Kolmogorov scaling. We refer to the simultaneous existence of BO and Kolmogorov scalings in the inertial range as the dual scaling of the BO phenomenology. The Bolgiano wave number $k_B \approx N^{3/2}\epsilon_u^{-5/4}\epsilon_b^{3/4}$ [2,17] is the wave number at which the KE spectrum shows demarcation from $k^{-11/5}$ to $k^{-5/3}$ scaling. For $k < k_B$, $E_u(k)$ is steeper than the Kolmogorov spectrum because buoyancy converts a significant part of KE into PE that leads to the attenuation of the KE flux $\Pi_u(k)$, which varies as $k^{-4/5}$ in the BO phenomenology. However, the PE flux $\Pi_b(k)$ is assumed to be constant. Bolgiano [17] and Obukhov [23] also argued that for $k > k_B$, buoyancy becomes negligible. Consequently, both the fluxes are constant and both spectra show Kolmogorov scaling for $k_B < k < k_{DI}$, where k_{DI} is the wave number at which the transition from the inertial range to the dissipation range occurs.

Several studies have been conducted to verify the phenomenology, but they failed to observe dual scaling. Kimura and Herring [24], and Kumar *et al.* [25] performed direct numerical simulation (DNS) of moderately SST at $\mathrm{Re} \approx 500$ and observed only BO scaling without a transition to the Kolmogorov scaling. Subsequently, the shell model results of Kumar and Verma [26] at $\mathrm{Re} = 1000$, theoretical analysis of Bhattacharjee [27,28], and scaling theory of Basu and Bhattacharjee [29] also showed only $k^{-11/5}$ scaling for the KE spectrum for moderate stratification. Large eddy simulation results of Agrawal and Chandy [30] also showed only the BO spectrum at moderate stratification. Note, however, that Rosenberg *et al.* [18] conducted a computational study of decaying rotating stratified turbulence at high Reynolds number and strong stratification ($\mathrm{Re} = 5.4 \times 10^4$, $\mathrm{Ri} = 1700$), and reported both the scaling regimes of the BO phenomenology in the inertial range.

Additionally, Alam *et al.* [31] and Bhattacharjee [32] studied moderately SST using the constancy of total energy flux $[\Pi_u(k) + \Pi_b(k)]$ under inviscid conditions. They observed $E_u(k) \sim k^{-5/3}$ and $E_b(k) \sim k^{-1/3}$ for $k \ll 1$, and $E_u(k) \sim k^{-11/5}$ and $E_b(k) \sim k^{-7/5}$ for $k \gg 1$, in their theoretical analysis. This observation shows that the regime of $k^{-5/3}$ scaling occurs at lower wave numbers than that for the $k^{-11/5}$ regime in the KE spectrum, which is in contrast to the predictions by Bolgiano [17] and Obukhov [23]. Therefore, the scaling regime of $k \ll 1$ needs to be investigated.

Alam *et al.* [31] also argued that the Kolmogorov scaling regime of the BO phenomenology could be observed in the numerical simulations when $k_d \gg k_B$, where k_d is the Kolmogorov wave number. Earlier numerical studies [24–26] did not have large enough Reynolds numbers, due to which $k_d/k_B \lesssim 2$. Thus, the dissipation effects become significant even at wave numbers only slightly larger than k_B ($k \gtrsim k_B$) and the $k^{-5/3}$ spectrum regime was not observed. Substitution of k_B and $k_d = (\epsilon_u/\nu^3)^{1/4}$ in the constraint $k_d \gg k_B$ yields the following condition [31]:

$$\epsilon_u \gg \frac{\mathrm{Ri}}{\sqrt{\mathrm{Re}}}\frac{U^3}{L}. \tag{1}$$

In this paper, one of our objectives is to demonstrate that SST flows indeed exhibit the dual scaling when the condition of Eq. (1) is fulfilled. However, the above condition requires a very large Re and Re_b, which are difficult to achieve in DNS. Therefore, we employ a shell model for simulating high Re flows.

For weak stratification, Wunsch and Kerstein [33], Kumar *et al.* [25], and Kumar and Verma [26] obtained $k^{-5/3}$ scaling in this regime. They argued that the $k^{-5/3}$ spectrum, akin to passive scalar turbulence, is a direct consequence of the fact that the buoyancy is negligible in comparison to the nonlinearity in weakly SST.

Nocturnal atmospheric flows are largely strongly stratified. In these flows, buoyancy suppresses the vertical motion of the fluid to a great extent; hence, the flow becomes quasi-two-dimensional and highly anisotropic [1,2,34,35]. In the absence of externally imposed vertical length scales, using theoretical arguments, Billant and Chomaz [36] proposed that the vertical integral length scale is of the order of the buoyancy length scale L_b, i.e., $L_v \approx L_b \approx U/N$; this proposition has been verified in many experimental [37–39] and numerical studies [22,40–42]. The buoyancy length scale represents the thickness of vertical shear layers [40], which is smaller for stronger stratification. Maffioli and Davidson [42] and Brethouwer *et al.* [22] reported that the horizontal integral length scale $L_h \approx U^3/\epsilon_u$. These results show that

$$\frac{L_v}{L_h} = \frac{U}{NL_h} = \frac{\epsilon_u^{1/3}}{NL_h^{2/3}} = \mathrm{Fr}_h, \tag{2}$$

where $\mathrm{Fr}_h \approx \mathrm{Fr}$ is the horizontal Froude number. In the limit of strong stratification, $\mathrm{Fr}_h \ll 1$, so $L_v/L_h \ll 1$. Thus, the vertical length scale is much smaller than the horizontal length scale for strongly stratified turbulence. Another fundamental length scale is the Ozmidov length scale $L_O = \sqrt{\epsilon_u/N^3}$. For scales smaller than L_O, flow is weakly affected by stratification and hence is isotropic. The ratio of L_v and L_O, and that of L_O and the Kolmogorov scale $L_K = (\nu^3/\epsilon_u)^{1/4}$, give

$$\frac{L_v}{L_O} = \mathrm{Fr}_h^{-1/2}, \quad \frac{L_O}{L_K} = \left(\frac{\epsilon_u}{\nu N^2}\right)^{3/4} = \mathrm{Re}_b^{3/4}. \tag{3}$$

So, as per Eq. (3), L_v and L_O are largely separated in the limit of $\mathrm{Fr}_h \ll 1$. Also, in order to ensure the scaling regime of isotropic turbulence for scales smaller than L_O, $\mathrm{Re}_b \gg 1$ is needed.

For $\mathrm{Fr}_h \ll 1$ and $\mathrm{Re}_b \gg 1$ concurrently, Billant and Chomaz [36] and Brethouwer *et al.* [22] predicted that the vertical KE and PE spectra should follow k_v^{-3} scaling for the length scales in the range (L_v, L_O), where k_v is the vertical wave number. For $\mathrm{Re}_b \approx 1$, DNS [22,43] and large-eddy simulation (LES) [30,44] studies obtained scaling that is consistent with the theoretically predicted k_v^{-3} scaling. However, the spectra were reported to be steeper [22,45] than k_v^{-3} for $\mathrm{Re}_b < 1$ and shallower [7,19,41,43,46] for $\mathrm{Re}_b > 10$. Augier *et al.* [46] and Maffioli [7], however, obtained k_v^{-3} scaling for $\mathrm{Re}_b > 10$ when considering the contribution of only large horizontal scales for computing the vertical spectra. For horizontal KE and PE spectra, a large body of literature [19,22,41–43,47–50] reported $k_h^{-5/3}$ scaling, where k_h is the horizontal wave number, in agreement with the classical Nastrom

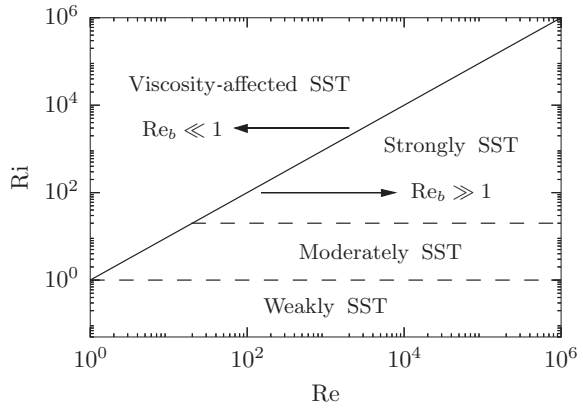

FIG. 1. Phase diagram of Ri vs Re for indicating the regimes of stably stratified turbulence.

and Gage spectra (Nastrom and Gage [51], Nastrom *et al.* [52]). Depending on Ri and Re, following Brethouwer *et al.* [22], we have shown the weakly, moderately, and strongly stratified regimes of SST in Fig. 1. The solid straight line corresponds to $\mathrm{Re}_b \approx \mathrm{ReFr}^2 \approx \mathrm{Re/Ri} = 1$, which separates the viscosity-affected and strong turbulence regimes of SST. The weakly and moderately stratified regimes are separated by $\mathrm{Ri} = 1$. Legaspi and Waite [53] showed that flow becomes anisotropic for $\mathrm{Fr} < 0.1$. So, based on $\mathrm{Ri} \approx \mathrm{Fr}^{-2}$ and accounting for some safety margin, we have selected $\mathrm{Ri} = 20$ as the threshold value for the demarcation between the moderately and strongly stratified regimes.

The above DNS studies focus on only the buoyancy-affected regime of strongly SST ($\mathrm{Fr}_h \ll 1$). But, the simultaneous existence of both buoyancy-affected and three-dimensional isotropic turbulence regimes requires $\mathrm{Re}_b \gg 1$, which is difficult to achieve in DNS with the current computational capacity. In this context, large-eddy simulation (LES) offers a promising alternative for simulating stratified flows at very high Reynolds numbers. In their LES results, Khani and Waite [54,55] showed the $k_h^{-5/3}$ spectra and reported that a resolution up to the buoyancy length scale was enough to sufficiently resolve the important properties of stratified turbulence. Scaling of the energy spectra has also been successfully reproduced in many other LES studies [30,44,56,57], and pancakelike structure and Kelvin-Helmholtz instabilities have also been observed.

Additionally, an important feature of stratified flows is the mixing across the stable density interfaces. Turbulent mixing has been studied extensively [12,39,42,43,58–60], but its accurate parametrization is still a major challenge in environmental fluid mechanics (Dauxois *et al.* [61]). Stratification affects the stirring and mixing processes, which are important in various phenomena such as dispersion of the pollutants, nutrients, and heat in the environment. According to Villermaux [62], turbulent mixing is the irreversible change of the physical properties of fluid parcels, specifically the scalar density. Since it is irreversible, mixing is associated with diffusive processes [15]. Recently, Jiang *et al.* [63] conducted an experimental study in a stratified inclined duct and explained the role of vortical motions in enhancing mixing by employing the recently developed "rortex-shear" decomposition [64,65] for splitting the vorticity vector into its pure rotational and shear components. They described how vortices stir the unmixed fluid into the mixing layer, generating strong small-scale density gradients. These gradients are then smoothed out by molecular diffusion (also, see Riley [66]). Mixing is quantified using mixing efficiency (η_{mix}), defined as [67,68]

$$\eta_{\mathrm{mix}} = \frac{\epsilon_b}{\epsilon_u + \epsilon_b}. \tag{4}$$

In oceans, Osborn [67] reported a nearly constant mixing efficiency $\eta_{\mathrm{mix}} \approx 0.17$ using oceanic measurements. Using numerical simulations, Venayagamoorthy and Stretch [68] and Portwood *et al.* [69,70] reported a similar value for mixing efficiency in sheared SST for $\mathrm{Ri} \approx 0.16$. In addition, the above authors [68–70] estimated mixing efficiency using theoretical arguments and proposed that $\eta_{\mathrm{mix}} \sim E_b/E_u$ at sufficiently high Reynolds number, where E_u and E_b are KE and PE, respectively.

Experimental studies by Turner [71], Kato and Phillips [72], and Holford and Linden [39], and computational study by Maffioli and Davidson [42], observed $\eta_{\mathrm{mix}} \sim \mathrm{Fr}^{-2}$ for homogeneous weakly stratified flows. Maffioli and Davidson [42] obtained similar scaling using theoretical arguments. For $\mathrm{Re} \gg 1$, they argued that

$$\epsilon_u \sim \frac{U^3}{L}, \quad \epsilon_b \sim \frac{U b_{\mathrm{rms}}^2}{L}, \quad -\overline{\mathcal{F}_B} \sim NU b_{\mathrm{rms}}, \tag{5}$$

where $-\overline{\mathcal{F}_B}$ is the mean buoyancy flux or the rate at which KE gets converted to PE due to buoyancy. Under the steady state, $-\overline{\mathcal{F}_B} = \epsilon_b$, which yields $b_{\mathrm{rms}} \sim NL$, so $\epsilon_b \sim N^2UL$. For weak stratification, $\epsilon_b \ll \epsilon_u$, and hence, $\eta_{\mathrm{mix}} \approx \epsilon_b/\epsilon_u \sim \mathrm{Fr}^{-2}$. However, the mixing efficiency is observed to be constant for strongly stratified flows [42,59,73,74]. Mukherjee and Balasubramanian [75,76] also reported that the mixing efficiency for strongly stratified lock-exchange gravity currents is constant for $\mathrm{Re}_b > 10$. The above studies focus on the weakly and strongly stratified regimes for the mixing efficiency. In this paper, we present the scaling of η_{mix} for the moderately stratified turbulence regime, which is the intermediate regime between the weakly and strongly stratified regimes.

Shell models are useful for simulating isotropic flows. Waite and Bartello [45], Kumar *et al.* [25], and Bhattacharjee *et al.* [77] have shown that the flows belonging to the weakly and moderately stratified regimes remain approximately isotropic. Therefore, in this paper, we present results in these regimes using a shell model.

In a shell model, the spectral space is divided into concentric shells, the radii of which increase exponentially (Ditlevsen [78]). The spectral velocity field, which is the mean velocity of all the modes present in a shell, is represented by a single complex variable. In the beginning, these low-dimensional models were extensively used to study the properties of homogeneous and isotropic hydrodynamic turbulence. Shell models reproduce interesting features, e.g., the Kolmogorov spectrum and the experimentally observed intermittency corrections for hydrodynamic turbulence [79–88]. Later, many shell models were developed to study buoyancy-driven flows [26,89–94] and magnetohydrodynamic turbulence [95–101]. Kumar and Verma [26], Brandenburg [89], Mingshun and Shida [90], Lozhkin and Frick [91], Olla [92], and Ching and Cheng

[93] constructed shell models for thermal convection and reported Kolmogorov-like scaling despite the differences in the formulations of nonlinear terms in their respective shell models. However, Suzuki and Toh [94] reported BO scaling for thermal convection. Kumar and Verma [26] also developed a shell model for stably stratified flows following the same formulations for nonlinear terms as that in thermal convection. In the present study, we adopt the shell model of Kumar and Verma [26] for simulations.

The outline of the paper is as follows: we describe the governing equations and shell model in Sec. II and present the simulation details in Sec. III. We discuss the temporal intermittency in KE and PE dissipation rates in Sec. IV. In Sec. V, we describe the transition from weak to moderate stratification and determine the critical Richardson number which separates the two regimes. In Sec. VI, we present the numerical results of the energy spectra and fluxes, and verify the BO phenomenology. We discuss the results for the scaling behavior of the mixing efficiency in Sec. VII. Finally, we conclude in Sec. VIII.

II. GOVERNING EQUATIONS

The evolution of velocity $[\mathbf{u} = (u_x, u_y, u_z)]$ and density fluctuations (b) for stably stratified flows under the Boussinesq approximation are described by the following set of equations [1,2,19,102,103]:

$$\frac{\partial \mathbf{u}}{\partial t} + (\mathbf{u}\cdot\boldsymbol{\nabla})\mathbf{u} = -\frac{1}{\rho_m}\boldsymbol{\nabla}\sigma - Nb\hat{\mathbf{z}} + \nu\nabla^2\mathbf{u} + \mathbf{F}_u, \quad (6)$$

$$\frac{\partial b}{\partial t} + (\mathbf{u}\cdot\boldsymbol{\nabla})b = Nu_z + \kappa\nabla^2 b, \quad (7)$$

$$\boldsymbol{\nabla}\cdot\mathbf{u} = 0, \quad (8)$$

where σ is the pressure field, $\mathbf{F}_u$ is the external force, $\hat{\mathbf{z}}$ is the vertical unit vector, $u_z = \mathbf{u}\cdot\hat{\mathbf{z}}$ is the vertical component of the velocity field, and N is the the Brunt-Väisälä frequency, which is defined as

$$N = \sqrt{\frac{g}{\rho_m}\left|\frac{d\bar{\rho}}{dz}\right|}, \quad (9)$$

where $|d\bar{\rho}/dz|$ is the background density gradient. Note that N is the natural frequency of internal gravity waves. Also, Eqs. (6) and (7) are coupled by buoyancy.

To simulate stably stratified turbulence, we employ a shell model [26,89–94] in which the governing equations are modeled as

$$\frac{du_n}{dt} = M_n(u,u) - Nb_n - \nu k_n^2 u_n + F_n, \quad (10)$$

$$\frac{db_n}{dt} = P_n(u,b) + Nu_n - \kappa k_n^2 b_n, \quad (11)$$

where u_n and b_n are the Fourier transforms of the velocity field and the density fluctuation, respectively, for the nth shell, $k_n = k_o\lambda^n$ is the wave number for the nth shell (where $\lambda > 1$ is the shell spacing), F_n is the external forcing term, and $M_n(u,u)$ and $N_n(u,b)$ are the nonlinear terms. We take $\lambda = 2$ for the present simulations. We employ the Sabra-based shell model (L'vov *et al.* [87]) developed by Kumar and Verma [26] for stratified flows in which the nonlinear terms are modeled as

$$M_n(u,u) = -i[a_1 k_n u_{n+1}^* u_{n+2} + a_2 k_{n-1} u_{n-1}^* u_{n+1} - a_3 k_{n-2} u_{n-1} u_{n-2}], \quad (12)$$

$$P_n(u,b) = -i[k_n(d_1 u_{n+1}^* b_{n+2} + d_2 b_{n+1}^* u_{n+2}) + k_{n-1}(d_3 u_{n-1}^* b_{n+1} + d_4 b_{n-1}^* u_{n+1}) + k_{n-2}(d_5 u_{n-1} b_{n-2} + d_6 b_{n-1} u_{n-2})], \quad (13)$$

where $\{a_1, a_2, a_3\}$ and $\{d_1, d_2, d_3, d_4, d_5, d_6\}$ are constant. Under the inviscid limit ($\nu = \kappa = 0$) and in the absence of the external force ($F_n = 0$), the total energy ($E_u + E_b$) and kinetic helicity are conserved for vanishing or periodic boundary condition [4,5]. These conservation laws yield the following conditions [26]:

$$\mathrm{Re}\left[\sum_n u_n^* M_n(u,u)\right] = 0, \quad (14)$$

$$\mathrm{Re}\left[\sum_n (-1)^n k_n u_n^* M_n(u,u)\right] = 0, \quad (15)$$

$$\mathrm{Re}\left[\sum_n b_n^* N_n(u,b)\right] = 0, \quad (16)$$

where Re stands for the real part. Constraints (14) and (15), respectively, lead to

$$a_1 + a_2 + a_3 = 0, \quad (17)$$

$$a_1 - a_2\lambda + a_3\lambda^2 = 0, \quad (18)$$

and constraint (16) yields

$$d_4 = -d_2, \quad d_5 = d_1, \quad d_6 = d_3. \quad (19)$$

In our simulations, in order to satisfy all the above conditions, we choose following values of the constants:

$$a_1 = \frac{\lambda}{\lambda - 1}, \; a_2 = -1.0, \; a_3 = -\frac{1}{\lambda - 1}, \quad (20)$$

$$d_1 = 5\lambda, \quad d_2 = -5\lambda, \quad d_3 = -\frac{5\lambda}{2}. \quad (21)$$

To supply energy into the system, we use the random external forcing $F_n = \eta_n e^{i\theta_n}$, where θ_n is the phase for the nth shell, which takes a random value in the interval $(0, 2\pi)$, and η_n is the forcing magnitude chosen in such a way that the KE supply rate ϵ_{inj} remains constant. This formalism of the forcing is motivated by the formulations of Maffioli [7] and Stepanov and Plunian [101]. The expression for η_n is given by

$$\eta_n = \frac{1}{dt}\left[-A_n \pm \sqrt{A_n^2 + \frac{2\epsilon_{\mathrm{inj}} dt}{n_f}}\right], \quad (22)$$

where $A_n = \mathrm{Re}(u_n e^{-i\theta_n})$, dt is the time step, and n_f is the total number of shells to be forced. Of the two values of η_n given by Eq. (22), we use the one with lower $|\eta_n|$ in our simulations so that the power input to the system is always positive [7]. The derivation of the expression is provided in the Appendix.

The dynamical equations for the total kinetic energy [$E_u = (1/2)\sum_n |u_n|^2$] and potential energy [$E_b = (1/2)\sum_n |b_n|^2$] are derived using Eqs. (10) and (11) as

$$\frac{dE_u}{dt} = \mathcal{F}_B(t) - D_u(t) + \mathcal{F}_u(t), \tag{23}$$

$$\frac{dE_b}{dt} = -\mathcal{F}_B(t) - D_b(t), \tag{24}$$

where $D_u(t)$ and $D_b(t)$ are, respectively, the KE and PE dissipation rates, $\mathcal{F}_u(t)$ is the KE injection rate by the external force, and $-\mathcal{F}_B(t)$ is the rate of conversion from KE to PE by buoyancy:

$$D_u(t) = \nu\left[\sum_n k_n^2 |u_n|^2\right], \tag{25}$$

$$D_b(t) = \kappa\left[\sum_n k_n^2 |b_n|^2\right], \tag{26}$$

$$\mathcal{F}_u(t) = \left[\sum_n \mathrm{Re}(F_u u_n^*)\right], \tag{27}$$

$$\mathcal{F}_B(t) = -N\left[\sum_n \mathrm{Re}(u_n b_n^*)\right]. \tag{28}$$

Under the statistically steady state ($dE_u/dt = 0$ and $dE_b/dt = 0$), Eqs. (23) and (24) simplify to the following (Verma [5,103]):

$$\epsilon_u - \overline{\mathcal{F}_B} = \epsilon_{\mathrm{inj}}, \tag{29}$$

$$\epsilon_b = -\overline{\mathcal{F}_B}, \tag{30}$$

where $\epsilon_u = \langle D_u \rangle$, $\epsilon_b = \langle D_b \rangle$, $\epsilon_{\mathrm{inj}} = \langle \mathcal{F}_u \rangle$, and $\overline{\mathcal{F}_B} = \langle \mathcal{F}_B \rangle$ are mean quantities. Note that $\langle \cdot \rangle$ denotes the time averaging. Equations (29) and (30) lead to

$$\epsilon_u + \epsilon_b = \epsilon_{\mathrm{inj}}. \tag{31}$$

Using Eq. (4), we write the mixing efficiency as

$$\eta_{\mathrm{mix}} = \frac{\epsilon_b}{\epsilon_{\mathrm{inj}}}. \tag{32}$$

It represents the fraction of the externally supplied kinetic energy that is used for the diffusion of the density fluctuations.

III. SIMULATION DETAILS

We perform simulations at different combinations of the energy supply rate and viscosity. At $\nu = \kappa = 10^{-5}$, we simulate for $\epsilon_{\mathrm{inj}} = \{0.25, 0.50, 0.75, 1.0, 1.75, 2.5\}$, and at $\epsilon_{\mathrm{inj}} = 1$, simulations are carried out for Prandtl number $\mathrm{Pr} = \nu/\kappa = 1$ with $\nu = \kappa = \{10^{-5}, 10^{-6}, 10^{-7}\}$. For each combination, we carry out numerical runs for various levels of stratification; N varies in the range $(0.1, 5.0)$. We also perform one run at larger viscosity ($\nu = \kappa = 10^{-3}$) and $\epsilon_{\mathrm{inj}} = 1$, $N = 5$. In total, we carry out 174 simulations and all are forced at $n = 0$ and $n = 1$, so $n_f = 2$. We employ the following boundary conditions:

$$u_{-2} = u_{-1} = b_{-2} = b_{-1} = 0, \tag{33}$$

$$u_{N_T} = u_{N_T+1} = b_{N_T} = b_{N_T+1} = 0, \tag{34}$$

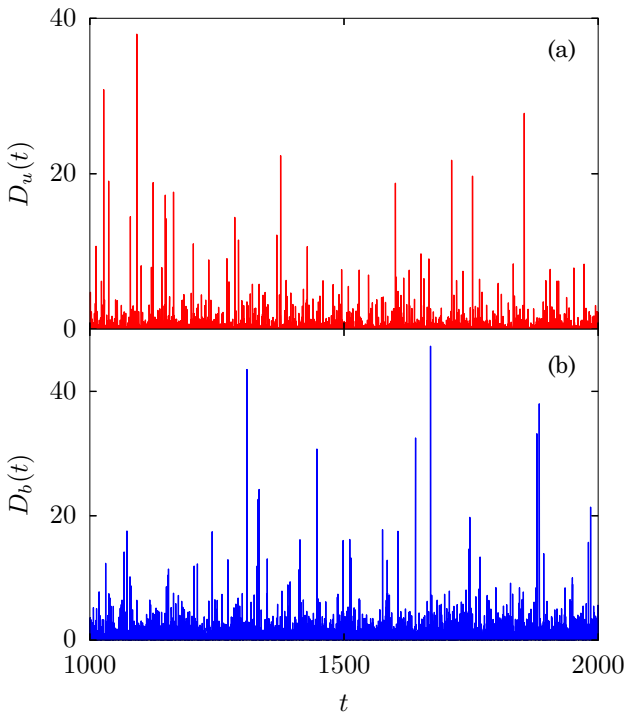

FIG. 2. For $\nu = \kappa = 10^{-6}$, $\epsilon_{\mathrm{inj}} = 1$, and $N = 5$, plots of the time evolution of the (a) kinetic energy dissipation rate $D_u(t)$ and (b) potential energy dissipation rate $D_b(t)$. The figures show extremely high intermittency.

where N_T is the total number of shells. We divide the wavenumber space into $N_T = 40$ shells. For time marching, we use the fourth-order Runge-Kutta (RK4) method with $dt = 10^{-5}$. We run each simulation for 2000 eddy turn over times, and average all computed quantities for 10 000 time frames of the last 1000 eddy turn over times. For each set of parameters, the computed quantities are further averaged over 16 independent simulations started with random initial conditions [104,105].

In the following sections, we discuss our simulation results.

IV. TEMPORAL INTERMITTENCY IN THE DISSIPATION RATES

In Fig. 2, we exhibit the time history of the instantaneous KE dissipation rate $D_u(t)$ and PE dissipation rate $D_b(t)$, for $\nu = \kappa = 10^{-6}$, $\epsilon_{\mathrm{inj}} = 1$, and $N = 5$. The figure illustrates intermittent events of extremely strong dissipation. This phenomenon is known as intermittency, which is one of the significant characteristics of turbulent flows. The emergence of the intermittent behavior is caused by the increasing non-Gaussian nature of the velocity and density fluctuations towards dissipation scales due to abrupt outbursts of massive energy arriving at these scales that eventually gets dissipated [78,88].

Intermittency can be quantified using the flatness of the velocity field $\mu_u(k)$ and density field $\mu_b(k)$, which are defined as (Biskamp [106], Biferale [88])

$$\mu_u(k_n) = \frac{\langle u_n^4 \rangle}{\langle u_n^2 \rangle^2}, \quad \mu_b(k_n) = \frac{\langle b_n^4 \rangle}{\langle b_n^2 \rangle^2}. \tag{35}$$

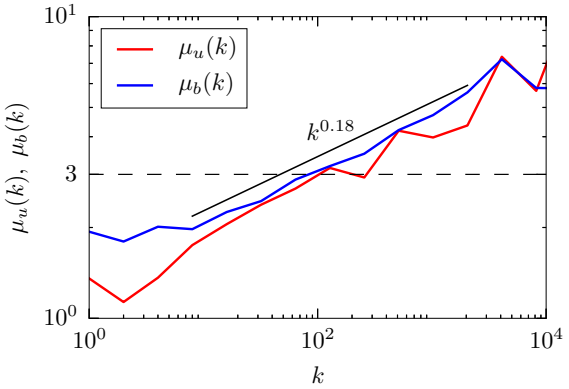

FIG. 3. For $\nu = \kappa = 10^{-6}$, $\epsilon_{\rm inj} = 1$, and $N = 5$, plots of the flatness of velocity $\mu_u(k)$ and density fluctuations $\mu_b(k)$. The black solid line is the reference line indicating $k^{0.18}$ scaling. The horizontal line is $\mu_u(k) = \mu_b(k) = 3$ for Gaussian signals.

We plot $\mu_u(k)$ and $\mu_b(k)$ for $N = 5$, $\nu = \kappa = 10^{-6}$, and $\epsilon_{\rm inj} = 1$ in Fig. 3. Note that flatness is 3 for a Gaussian signal and any deviation from 3 indicates non-Gaussianity. The figure shows that $\mu_u(k)$ and $\mu_b(k)$ are less than 3 for $k \lesssim 100$ and greater than 3 for $k \gtrsim 100$. Also, $\mu_u(k)$ and $\mu_b(k)$ increase monotonically with wave number and follow $k^{0.18}$ scaling. This increase with wave number shows that the velocity and density fluctuations exhibit an increased non-Gaussian nature at smaller scales, which implies strong intermittency towards the dissipation scales. In comparison, for hydrodynamic turbulence, earlier investigations [83,107–110] reported scaling of $\mu_u(k)$ from $k^{0.10}$ to $k^{0.16}$. Our result provides a slightly steeper scaling in SST.

Using $D_u(t)$ and $D_b(t)$ time signals, we compute the mean energy dissipation rates, ϵ_u and ϵ_b, by averaging the signals in the time interval (1000, 2000). We find that the total energy dissipation rate equals the energy supply rate, i.e., $\epsilon_u + \epsilon_b = \epsilon_{\rm inj}$. The same is true for other simulations as well. Thus, it shows that our simulations have attained a statistical steady state.

In the next section, we discuss the transition from weak to moderate stratification and compute the critical Richardson number at which this transition occurs.

V. TRANSITION FROM WEAK TO MODERATE STRATIFICATION: DETERMINATION OF CRITICAL RICHARDSON NUMBER

In the limit of weakly stratified turbulence, Maffioli and Davidson [42] analytically derived that $b_{\rm rms} \propto N$, where

$$b_{\rm rms} = \left\langle \sum_n |b_n|^2 \right\rangle^{1/2}. \tag{36}$$

In Fig. 4, we numerically verify that $b_{\rm rms} \sim N$ holds up to a certain N and then a transition occurs to nearly $b_{\rm rms} \sim N^{1/2}$ on further increase of stratification. The slowdown of the rate of increase of $b_{\rm rms}$ with the level of stratification is also reported by Mohapatra *et al.* [34,111]. The critical Brunt-Väisälä frequency N_c, after which $b_{\rm rms}$ deviates from the linear scaling, demarcates the weak and moderate stratification.

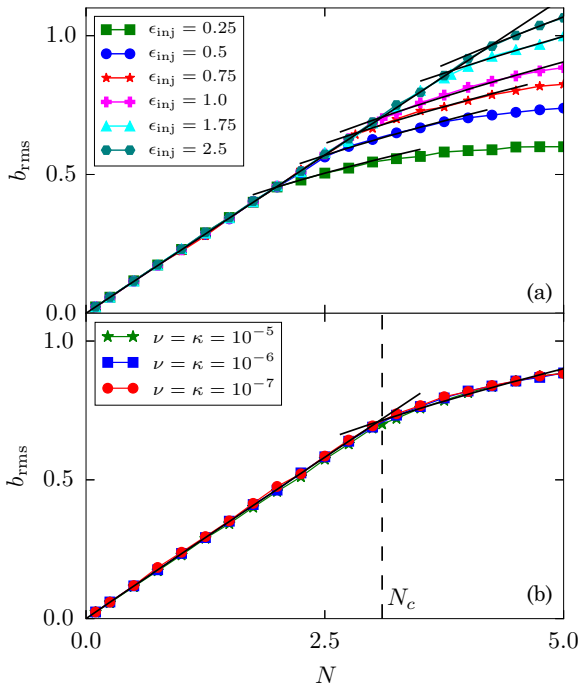

FIG. 4. Plots of the rms density fluctuations $b_{\rm rms}$ vs N (a) for different $\epsilon_{\rm inj}$ at $\nu = \kappa = 10^{-5}$ and (b) for different $\nu = \kappa$ at $\epsilon_{\rm inj} = 1.0$. $b_{\rm rms}$ depends upon N but not ν. The curves in both figures are the fit to the data. For weakly SST, $b_{\rm rms} \sim N$, and for moderately SST, $b_{\rm rms}$ nearly follow $N^{1/2}$ scaling. The vertical line in (b) is $N = N_c = 3.11$.

Figure 4(a) shows that N_c increases with the increase of $\epsilon_{\rm inj}$. We provide N_c and the scaling relations of $b_{\rm rms}$ for different $\epsilon_{\rm inj}$ at $\nu = \kappa = 10^{-5}$ in Table I. We also observe that for a given $\epsilon_{\rm inj}$, $b_{\rm rms}$ remains unchanged as ν varies, as shown in Fig. 4(b). It implies that N_c depends on $\epsilon_{\rm inj}$, but not ν or κ. Using curve fitting, we find that N_c convincingly follows $N_c = 3.13\epsilon_{\rm inj}^{1/3}$, as shown in Fig. 5. In order to determine the critical Richardson number Ri_c, we run simulations for different pairs of N_c and the corresponding $\epsilon_{\rm inj}$ (see Table I). We substitute

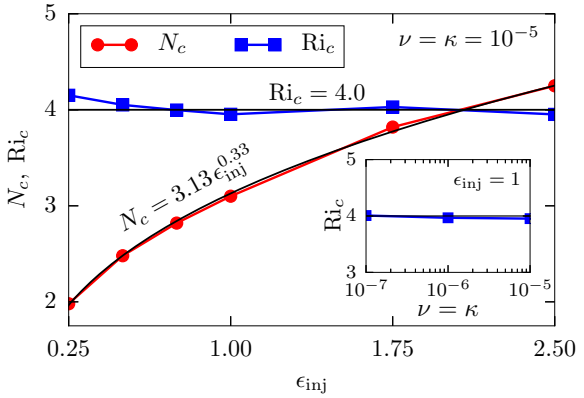

FIG. 5. For $\nu = \kappa = 10^{-5}$, plots of the critical Richardson number Ri_c and critical Brunt-Väisälä frequency N_c vs $\epsilon_{\rm inj}$. Inset: Ri_c vs $\nu = \kappa$ for $\epsilon_{\rm inj} = 1$. The black curve, $N_c = 3.13\epsilon_{\rm inj}^{0.33}$, is the fit to the data, and the horizontal lines in the figure and inset are $\mathrm{Ri}_c = 4.0$.

TABLE I. For various $\epsilon_{\rm inj}$ at $\nu = \kappa = 10^{-5}$, the critical Brunt-Väisälä frequency (N_c) and the scaling relations of $b_{\rm rms}$ for $N \lesssim N_c$ and $N \gtrsim N_c$ are shown.

$\epsilon_{\rm inj}$	N_c	Scaling relation for $N \lesssim N_c$	Scaling relation for $N \gtrsim N_c$
0.25	1.98	$b_{\rm rms} = (0.230 \pm 0.001)N^{0.997\pm0.003}$	$b_{\rm rms} = (0.329 \pm 0.004)N^{0.467\pm0.008}$
0.50	2.48	$b_{\rm rms} = (0.228 \pm 0.001)N^{0.995\pm0.003}$	$b_{\rm rms} = (0.364 \pm 0.021)N^{0.489\pm0.025}$
0.75	2.82	$b_{\rm rms} = (0.227 \pm 0.002)N^{0.999\pm0.004}$	$b_{\rm rms} = (0.393 \pm 0.021)N^{0.484\pm0.021}$
1.00	3.11	$b_{\rm rms} = (0.229 \pm 0.001)N^{0.998\pm0.001}$	$b_{\rm rms} = (0.394 \pm 0.022)N^{0.508\pm0.020}$
1.75	3.82	$b_{\rm rms} = (0.230 \pm 0.001)N^{0.991\pm0.002}$	$b_{\rm rms} = (0.451 \pm 0.065)N^{0.494\pm0.049}$
2.50	4.25	$b_{\rm rms} = (0.230 \pm 0.001)N^{0.995\pm0.002}$	$b_{\rm rms} = (0.399 \pm 0.073)N^{0.611\pm0.059}$

$b_{\rm rms}$,

$$U = \left\langle \sum_n |u_n|^2 \right\rangle^{1/2} \quad \text{and} \quad L = \frac{4\pi}{U^2} \sum_n \left[\frac{E_u(k_n)}{k_n} \right], \tag{37}$$

in Eq. (1) to compute Ri_c. We plot the variation of Ri_c with $\epsilon_{\rm inj}$ in Fig. 5 and the variation of the same with $\nu = \kappa$ in the inset. The figure shows that $\mathrm{Ri}_c \approx 4.0$ is almost independent of $\epsilon_{\rm inj}$ and ν (or κ, as $\mathrm{Pr} = 1$). Thus, our numerical results show that the transition from weak to moderate stratification occurs at $\mathrm{Ri} = \mathrm{Ri}_c \approx 4.0$. In Fig. 6, we plot instantaneous $\mathcal{F}_B$ [Eq. (28)] for various N (or Ri) at $\epsilon_{\rm inj} = 1.0$ and $\nu = \kappa = 10^{-6}$. The figure shows that for $N \leqslant 3$ ($\mathrm{Ri} \leqslant 3.75$), $\mathcal{F}_B < 0$ most of the time. It shows that the net conversion of kinetic energy to potential energy take place almost at every instant of time, and the instances of net transformation of the potential energy to kinetic energy are rare. However, in the case of $N = 4$ ($\mathrm{Ri} = 5.55$) or $N = 5$ ($\mathrm{Ri} = 6.84$), the excursions of $\mathcal{F}_B > 0$ are stronger and they occur more often, indicating that the potential energy also gets converted into kinetic energy quite often for these cases.

To support the above observation, we compute the probability $P_+(\mathcal{F}_B)$ of occurrence of the excursions of $\mathcal{F}_B > 0$, which is defined as

$$P_+(\mathcal{F}_B) = \frac{\text{No. instances of } \mathcal{F}_B > 0}{\text{Total no. instances}}, \tag{38}$$

where the total number of instances is 10 000. We plot $P_+(\mathcal{F}_B)$ vs Ri for different $\epsilon_{\rm inj}$ at $\nu = \kappa = 10^{-5}$ in Fig. 7. The figure shows that $P_+(\mathcal{F}_B)$ for various energy supply rates collapse to a single curve. The figure also shows that for $\mathrm{Ri} \lesssim \mathrm{Ri}_c \approx 4.0$, $P_+(\mathcal{F}_B)$ is very small and constant, but increases rapidly when $\mathrm{Ri} \gtrsim \mathrm{Ri}_c$ for all runs. As a result, it can be deduced that the instances of net conversion of PE to KE are insignificant in the limit of weakly stratified turbulence (for $\mathrm{Ri} \lesssim \mathrm{Ri}_c$); however, the net transformation of both energies into one another takes place more frequently for $\mathrm{Ri} \gtrsim \mathrm{Ri}_c$.

In the next section, we show that the energy spectra and fluxes satisfy the BO phenomenology for moderate stratification.

VI. NUMERICAL VERIFICATION OF THE BO PHENOMENOLOGY

We compute the averaged KE and PE spectra, and the corresponding fluxes as follows (Verma [103]):

$$E_u(k_n) = \frac{\langle |u_n|^2 \rangle}{2k_n}, \tag{39}$$

$$E_b(k_n) = \frac{\langle |b_n|^2 \rangle}{2k_n}, \tag{40}$$

$$\Pi_u(k_n) = a_3 k_{n-1} \langle \mathrm{Im}(u^*_{n-1} u^*_n u_{n+1}) \rangle - a_1 k_n \langle \mathrm{Im}(u^*_n u^*_{n+1} u_{n+2}) \rangle, \tag{41}$$

$$\Pi_b(k_n) = -d_1 k_n \langle \mathrm{Im}(b^*_n u^*_{n+1} b_{n+2}) \rangle - d_2 k_n \langle \mathrm{Im}(b^*_n b^*_{n+1} u_{n+2}) \rangle - d_1 k_{n-1} \langle \mathrm{Im}(b^*_{n-1} u^*_n b_{n+1}) \rangle - d_3 k_{n-1} \langle \mathrm{Im}(u^*_{n-1} b^*_n b_{n+1}) \rangle, \tag{42}$$

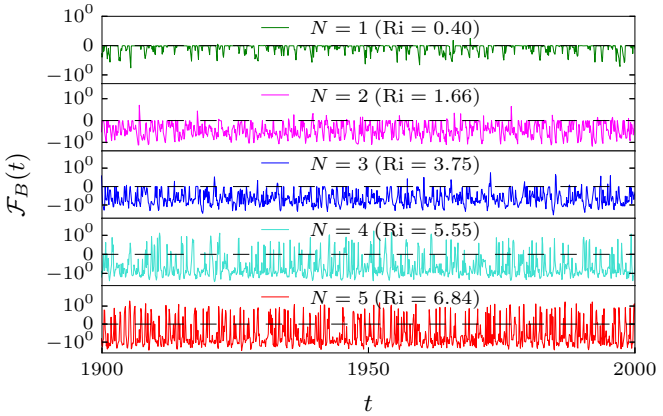

FIG. 6. For $\epsilon_{\rm inj} = 1.0$ and $\nu = \kappa = 10^{-6}$, plots of the time evolution of $\mathcal{F}_B(t)$ for various strengths of stratification.

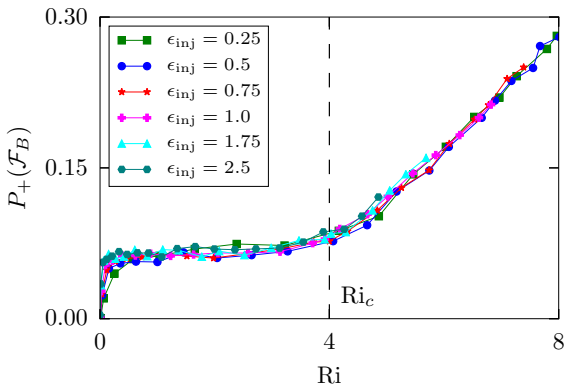

FIG. 7. For $\nu = \kappa = 10^{-5}$, plots of the probability density functions $P_+(\mathcal{F}_B)$ vs Ri for various energy supply rates.

TABLE II. The parameters for varying Brunt-Väisälä frequency (N) at $\epsilon_{\rm inj} = 1$: kinematic viscosity (ν), Richardson number (Ri), Reynolds number (Re), Bolgiano wave number (k_B), Kolmogorov wave number (k_d), and $\epsilon_u/[(\mathrm{Ri}/\sqrt{\mathrm{Re}})(U^3/L)]$. We take Prandtl number $\mathrm{Pr} = \nu/\kappa = 1$.

N	ν	Ri	Re	k_B	k_d	$\epsilon_u/[(\mathrm{Ri}/\sqrt{\mathrm{Re}})(U^3/L)]$
1.0	10^{-6}	0.40 ± 0.13	6.33×10^6	0.20	3.09×10^4	5.83×10^3
3.0	10^{-6}	3.75 ± 1.18	5.51×10^6	11	2.51×10^4	2.99×10^2
5.0	10^{-6}	6.84 ± 2.66	5.24×10^6	53	2.20×10^4	8.40×10^1
5.0	10^{-3}	6.54 ± 0.36	5.04×10^3	76	1.17×10^2	2.25

where Im denotes the imaginary part. We also compute k_B and k_d, and find that $k_B \ll k_d$ for all the high Reynolds number runs ($\mathrm{Re} \sim 10^6$), which implies that

$$\epsilon_u / \left(\frac{\mathrm{Ri}}{\sqrt{\mathrm{Re}}} \frac{U^3}{L} \right) \gg 1$$

(see Table II). Hence, the condition of Eq. (1) for the existence of dual scaling is satisfied.

To verify the BO phenomenology, we plot the energy spectra and fluxes in Fig. 8 for different levels of stratification ($N = 1, 3, 5$), keeping $\nu = \kappa = 10^{-6}$ and $\epsilon_{\rm inj} = 1$. In the figure, the vertical lines depict k_B and k_d for the three values of N. For $N = 1$, we find that $k_B < 1$ and it is therefore not indicated. Note that $k_B \ll k_d$ for all the runs presented. For $N = 5$, we observe that the energy spectra show evidence for the existence of $E_u(k) \sim k^{-11/5}$, $E_b(k) \sim k^{-7/5}$, and $\Pi_u(k) \sim k^{-4/5}$ for $k < k_B$. However, as k_B is only 53, which is too small, the BO scaling is only present for a short wave-number range. In this regime, the attenuation in $\Pi_u(k)$ is due to the conversion of KE to PE via buoyancy. Consequently, the KE spectrum becomes steeper than that predicted by the Kolmogorov theory. Also, Alam *et al.* [31], and Verma [4] showed that $\Pi_u(k) + \Pi_b(k) = \text{const}$ in the inertial range, so the decrease of $\Pi_u(k)$ with k yields a slight increase of $\Pi_b(k)$, as shown in Fig. 8(d). For $k > k_B$, buoyancy becomes negligible, and the conversion of KE to PE is insignificant. As a result, both spectra show $k^{-5/3}$ scaling for $k_B < k < k_{DI}$, and the fluxes are constant. Thus, our numerical results show some evidence of the validity of the dual scaling predicted by Bolgiano [17] and Obukhov [23]. However, for attaining a larger range of the BO spectrum, along with the condition of Eq. (1), some other approaches needs to be explored. One alternative is to consider the nonlocal transfer of energy by the Fourier modes in the shell model, as studied by Stepanov and Plunian [112] for magnetohydrodynamics. Rosenberg *et al.* [18] also reported BO scaling for a very narrow wave-number band in their numerical simulations of rotating stratified turbulence.

Under weak stratification ($N = 1$), the effect of the density field on the velocity field is negligible. In addition, $k_B < 1$, which is reported in Table II. Therefore, $E_u(k)$ and $E_b(k)$ fit better with the Kolmogorov scaling, and $\Pi_u(k)$ and $\Pi_b(k)$ are constant in the inertial range. However, at very large scales,

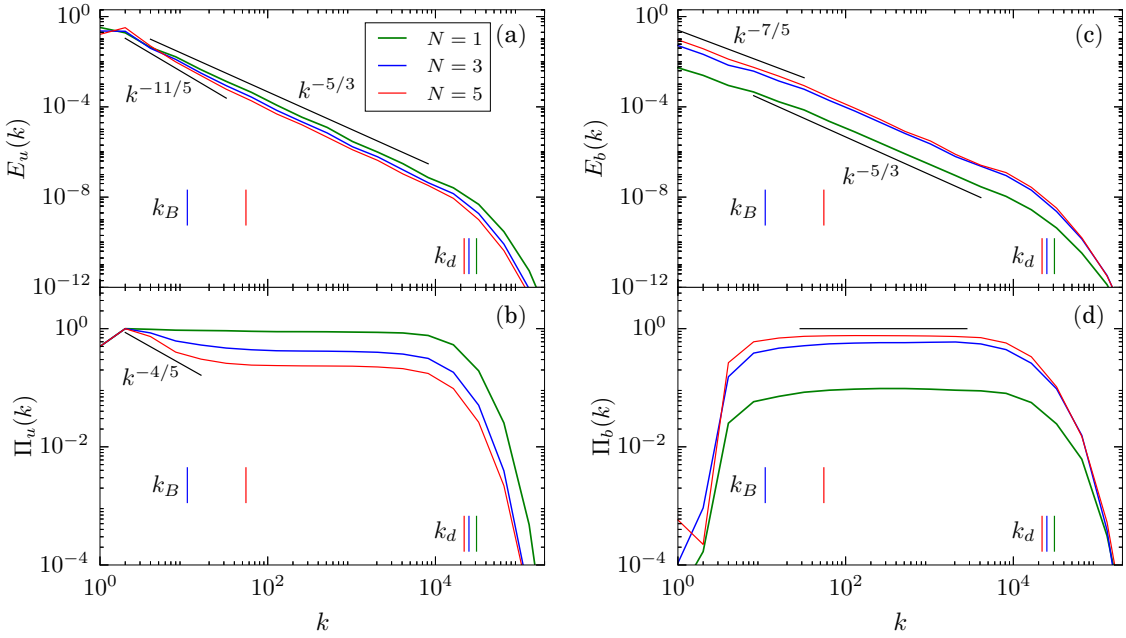

FIG. 8. For various strengths of stratifications, plots of the (a) KE spectrum $E_u(k)$, (b) KE flux $\Pi_u(k)$, (c) PE spectrum $E_b(k)$, and (d) PE flux $\Pi_b(k)$. For $N = 5$, the spectra and fluxes fit better with the the BO scaling for $k < k_B$ and with the Kolmogorov scaling for $k > k_B$ in the inertial range. For $N = 1$, the spectra and fluxes fit better with the Kolmogorov scaling throughout the inertial range. The black solid lines are for reference to visualize scalings. k_B and k_d for different values of N have been indicated by the vertical lines. For $N = 1$, $k_B < 1$, so it is not shown. Here, $\nu = \kappa = 10^{-6}$ and $\epsilon_{\rm inj} = 1.0$.

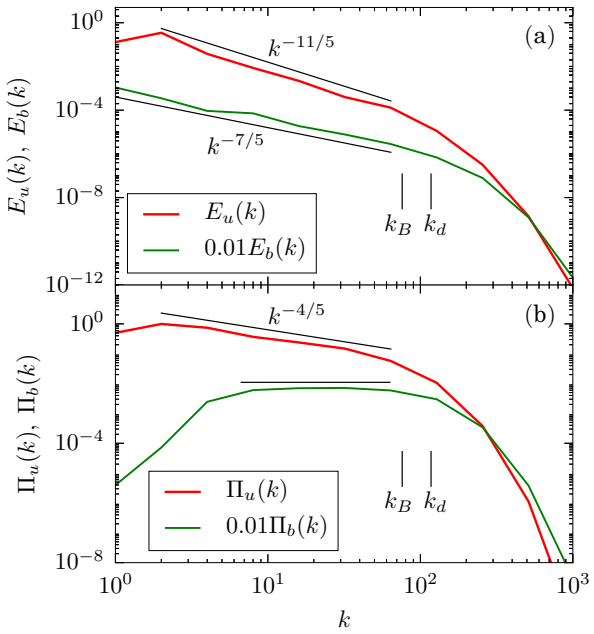

FIG. 9. For $N = 5$, $\nu = \kappa = 10^{-3}$, and $\epsilon_{\text{inj}} = 1.0$, plots of (a) the KE spectrum $E_u(k)$ and PE spectrum $E_b(k)$, and (b) the KE flux $\Pi_u(k)$ and PE flux $\Pi_b(k)$. The spectra and flux exhibit only the BO scaling in the inertial range. The black solid lines are for reference to visualize scalings. The vertical lines correspond to $k_B = 76$ and $k_d = 117$.

$E_b(k)$ is a bit shallower than the Kolmogorov spectrum, as shown in Fig. 8(c). It is possibly due to a marginal increase in $\Pi_b(k)$ due to the transfer of kinetic energy to potential energy; however, this transfer is very small as $\Pi_b(k) \ll \Pi_u(k)$. Our observations are consistent with those of Wunsch and Kerstein [33], Kumar *et al.* [25], and Basu and Bhattacharjee [29].

In Fig. 8, we also plot the energy spectra and fluxes for $N = 3$, close to N_c at which the transition from weakly to moderately SST takes place. For this case, at large scales, $E_u(k)$ exhibits scaling between $k^{-5/3}$ and $k^{-11/5}$, and the depletion of $\Pi_u(k)$ is shallower than $k^{-4/5}$. Also, $\Pi_b(k)$ increases marginally as the total energy flux is constant. But, $E_b(k)$ shows $k^{-7/5}$ scaling. Thus, buoyancy is not negligible, but at the same time it is not strong enough for the kinetic energy to show the BO spectrum.

Now, to verify that the Kolmogorov scaling is absent for moderately SST when the condition of Eq. (1) is not satisfied, we simulate the flow at a smaller Reynolds number (last simulation in Table II). We find that $\text{Re} = 5.04 \times 10^3$ and

$$\epsilon_u / \left(\frac{\text{Ri}}{\sqrt{\text{Re}}} \frac{U^3}{L} \right) = 2.25.$$

Hence, following Eq. (1), we conclude that k_B and k_d are of the same order. Figure 9 illustrates the energy spectra and fluxes for this case. It is evident from the figure that the energy spectra and fluxes show only the BO scaling; $E_u(k)$ and $E_b(k)$ follow $k^{-11/5}$ and $k^{-7/5}$ scalings, respectively [Fig. 9(a)], $\Pi_b(k)$ is constant, and $\Pi_u(k)$ fits quite well with $k^{-4/5}$, as shown in Fig. 9(b). However, there is no transition to the Kolmogorov scaling because k_d is not much bigger than k_B as the condition of Eq. (1) is not fulfilled. The DNS of

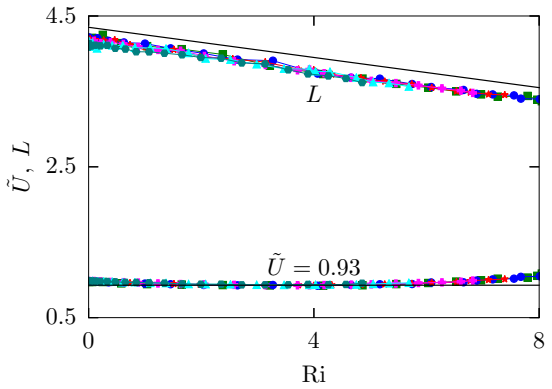

FIG. 10. For $\nu = \kappa = 10^{-5}$, plots of integral length scale L and normalized rms velocity $\tilde{U} = U/(\epsilon_{\text{inj}} L)^{1/3}$ vs Ri for various ϵ_{inj}. Legend is the same as that of Fig. 7. The straight line is $L = 4.35 - 0.1\text{Ri}$.

Kumar *et al.* [25], LES of Agrawal and Chandy [30], and shell model of Kumar and Verma [26] for moderately SST at $\text{Re} \approx 10^3$ also show the existence of only the $k^{-11/5}$ spectrum; therefore, our results are in good agreement with their results. We find that $k_B = 76$ and $k_d = 117$, and hence buoyancy is active throughout the inertial range for this case. Therefore, the dual scaling is not obtained for this case.

In the following section, we discuss the mixing efficiency. We start with the variation of the rms velocity and integral length scale with the strength of stratification.

VII. SCALING OF THE MIXING EFFICIENCY

We plot the integral length scale L and normalized rms velocity $\tilde{U} = U/(\epsilon_{\text{inj}} L)^{1/3}$ vs Ri in Fig. 10. As is evident from the figure, both L and $\tilde{U}$ are independent of ϵ_{inj}. Lindborg [19] and Maffioli [7] claimed that $L \approx 2\pi/k_f$, where k_f is the forcing wave number. We forced the system at $k = 1, 2$ with equal energy for all the simulations, so $k_f \approx 1.5$ for all our runs. Substitution of $k_f = 1.5$ in $L \approx 2\pi/k_f$ yields $L \approx 4.2$. The figure shows that L is approximately equal to 4.2 for very small Ri's, but it decreases linearly as Ri increases. In addition, as shown in the figure, $\tilde{U} \approx 0.93$ is almost independent of the level of stratification, which implies that U varies as

$$U = 0.93(\epsilon_{\text{inj}} L)^{1/3}. \tag{43}$$

In Fig. 11, we plot η_{mix} vs Ri and find that η_{mix} for different ϵ_{inj} follow the same curve. We use curve fitting to derive the scaling relation of η_{mix}. We observe that η_{mix} increases almost linearly with Ri for weakly stratified turbulence as

$$\eta_{\text{mix}} = (0.221 \pm 0.011)\text{Ri}^{0.960 \pm 0.012} \quad \text{for} \quad \text{Ri} \lesssim \text{Ri}_c, \tag{44}$$

as shown in the figure, consistent with the earlier findings [39,42,71,72]. For $\text{Ri} \gtrsim \text{Ri}_c$ (moderate stratification), η_{mix} deviates from the linear scaling and the rate of increase becomes slower. Using curve fitting, we find that

$$\eta_{\text{mix}} = (0.398 \pm 0.035)\text{Ri}^{0.344 \pm 0.03} \quad \text{for} \quad \text{Ri} \gtrsim \text{Ri}_c, \tag{45}$$

as shown in the inset of the figure. A possible reason for this slowdown is the rapid increase of occurrence of the instances

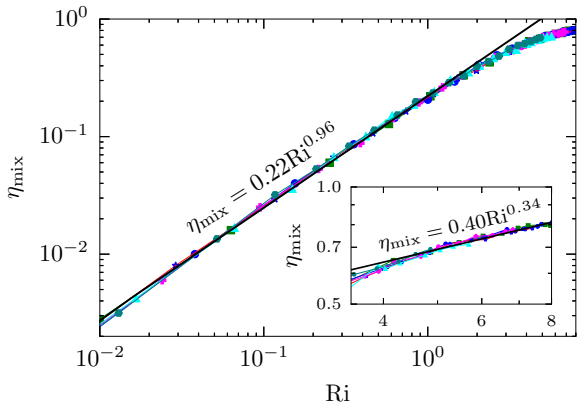

FIG. 11. For $\nu = \kappa = 10^{-5}$, plots of the mixing efficiency $\eta_{\rm mix}$ vs Ri for various $\eta_{\rm mix}$. Inset: the same plots for Ri $\geqslant 3.5$. The curves represent the fits to the data. Legend is the same as that of Fig. 7.

of the net conversion of PE to KE for Ri $\gtrsim {\rm Ri}_c$ (explained in Sec. V), which effectively slows down the growth rate of $\epsilon_b = \overline{\mathcal{F}_B}$, and hence $\eta_{\rm mix}$. For strongly SST, many recent studies [42,59,74] reported that $\eta_{\rm mix} = $ const. Unfortunately, we cannot simulate the flow at strong stratification because the flow then becomes anisotropic and our shell model needs major modification.

In short, we observe that $\eta_{\rm mix} \sim {\rm Ri}$ for weakly SST, while for moderately SST, it scales as $\eta_{\rm mix} \sim {\rm Ri}^{\alpha}$, with $\alpha \approx 1/3$. We conclude the paper in the following section.

VIII. CONCLUSIONS

In this work, we perform shell model simulations for stably stratified flow for various pairs of energy supply rate and viscosity in weakly and moderately stratified regimes at unitary Prandtl number. Here, we fulfill three objectives: (i) we find the critical Brunt-Väisälä frequency N_c and Richardson number ${\rm Ri}_c$ at which changeover from weak to moderate stratification takes place, (ii) we present numerical results that suggest the potential validation of the Bolgiano-Obukhov phenomenology, and (iii) we obtain scaling relations for mixing efficiency.

For finding N_c and ${\rm Ri}_c$, we use the observation that density fluctuations $b_{\rm rms}$ vary linearly with N for weakly stratified turbulence [42], i.e., $b_{\rm rms}$ deviates from the linear scaling at $N = N_c$ (or Ri $= {\rm Ri}_c$). These critical values demarcate weakly from moderately stratified regimes of SST. We observe that N_c increases with the energy supply rate $\epsilon_{\rm inj}$ as $N_c \sim \epsilon_{\rm inj}^{1/3}$, but does not depend on viscosity ν, while ${\rm Ri}_c \approx 4$ is independent of both $\epsilon_{\rm inj}$ and ν. For weakly stratified turbulence (Ri $\lesssim {\rm Ri}_c$), we observe that instances of net conversion of the potential energy to kinetic energy are rare. For Ri $\gtrsim {\rm Ri}_c$, the frequency of such instances increases rapidly. Note, however, that the time-averaged conversion is always from kinetic energy to potential energy.

For moderately stably stratified turbulence, our numerical analysis provides some preliminary evidence in favor of the dual scaling spectrum of the Bolgiano-Obukhov (BO) phenomenology. The BO phenomenology predicts that the kinetic and potential energy spectra, respectively, follow $k^{-11/5}$ and $k^{-7/5}$ scaling for $k < k_B$, where k_B is the Bolgiano wave number. For $k > k_B$, the energy spectra follow $k^{-5/3}$ scaling. To date, however, the dual scaling is not observed. Alam *et al.* [31] derived a condition for the existence of $k^{-5/3}$ scaling in the inertial range for $k > k_B$. The condition yields $\epsilon_u \gg ({\rm Ri}/\sqrt{\rm Re})(U^3/L)$, which requires high Reynolds number. In the present paper, we satisfy the above condition in our shell model simulations and observe that both energy spectra exhibit the dual scaling. However, the range of $E_u(k) \sim k^{-11/5}$ and $E_b(k) \sim k^{-7/5}$ spectra that we obtained is not large enough and more investigation is needed to establish a larger wave-number band for the BO scaling. Note that the above condition is difficult to obtain in direct numerical simulations.

Furthermore, we obtain the scaling relations for the mixing efficiency. We observe that the mixing efficiency increases linearly with Ri for Ri $\lesssim {\rm Ri}_c$, but slows down to ${\rm Ri}^{1/3}$ for Ri $\gtrsim {\rm Ri}_c$ in moderately SST. This changeover of scaling is possibly due to the slowdown of the transfer rate from the kinetic energy to potential energy.

Nocturnal atmospheric flows experience strong stratification that suppresses the vertical motion and makes the flows highly anisotropic. Currently, our shell model does not have the ability to capture the anisotropic effects. As a result, the present study does not focus on strongly SST. However, motivated by the shell models of Gürcan and Grappin [113] and Carbone and Veltri [114], which incorporate angular dependence to capture anisotropy, we plan to modify our shell model solver to study strongly stratified turbulence in a future study. Finally, we reiterate that the results presented in this paper may not be applicable for very large Richardson numbers and fluids of large Prandtl numbers for which stable density layers with sharp interfaces form.

ACKNOWLEDGMENTS

The authors thank Anirban Guha, Shashwat Bhattacharya, Manohar Sharma, Mohammad Anas, Soumyadeep Chatterjee, and Roshan Samuel for useful discussions. This work was supported by the research Grant No. PHY/DST/2020455 from the Department of Science and Technology (DST), India. Our numerical simulations were performed on HPC2013, and the Taylor and Chaos clusters of IIT Kanpur, India.

APPENDIX: ENERGY SUPPLY RATE FROM THE RANDOM FORCING

We use the random forcing ($F_n = \eta_n e^{i\theta_n}$) to supply the kinetic energy into the system. We evaluate the expression for η_n by considering the simplest form of the shell model equation (excluding the nonlinear and dissipative terms) as

$$\frac{\partial u_n(t)}{\partial t} = F_n(t). \tag{A1}$$

The corresponding discretization of Eq. (A1) for time evolution is

$$\frac{u_n(t+dt) - u_n(t)}{dt} = \eta_n e^{i\theta_n}. \tag{A2}$$

Using Eq. (A2), we can easily arrive at the following equation:

$$\frac{1}{2}\left(\frac{|u_n(t+dt)|^2-|u_n(t)|^2}{dt}\right)=\eta_n \mathrm{Re}[u(t)e^{-i\theta_n}]+\frac{1}{2}\eta_n^2 dt. \tag{A3}$$

If ϵ and n_f are, respectively, the energy supply rate and the number of shells to be forced, we can write

$$\frac{\epsilon_{\mathrm{inj}}}{n_f}=\frac{1}{2}\left[\frac{|u_n(t+dt)|^2-|u_n(t)|^2}{dt}\right]. \tag{A4}$$

Equations (A3) and (A4) yield the following:

$$\eta_n^2+\left(\frac{2A_n}{dt}\right)\eta_n-\left(\frac{2\epsilon_{\mathrm{inj}}}{n_f dt}\right)=0, \tag{A5}$$

where $A_n=\mathrm{Re}[u(t)e^{-i\theta_n}]$ and the solution of Eq. (A5) is

$$\eta_n=\frac{1}{dt}\left[-A_n\pm\sqrt{A_n^2+\frac{2\epsilon_{\mathrm{inj}}dt}{n_f}}\right]. \tag{A6}$$

The energy injection rate to the nth shell $\mathcal{F}_n$ due to the external random force is $\mathcal{F}_n=\mathrm{Re}(u_nF_n^*)=\eta_nA_n$ [equal to the first term on the right-hand side of Eq. (A3)]. However, some artificial energy also gets injected into the shell because of the discretization error. The artificial energy is equal to $(1/2)\eta_n^2dt$ [the second term on the right-hand side of Eq. (A3)]. To minimize the artificial energy injection and to ensure that $\mathcal{F}_n$ is always positive, we use η_n which has a lower magnitude ($|\eta_n|$) of the two values of η_n given by (A6) in our simulations [7].

[1] P. A. Davidson, *Turbulence in Rotating, Stratified and Electrically Conducting Fluids* (Cambridge University Press, Cambridge, 2013).
[2] M. K. Verma, *Physics of Buoyant Flows: From Instabilities to Turbulence* (World Scientific, Singapore, 2018).
[3] E. Deusebio, P. Augier, and E. Lindborg, J. Fluid Mech. **755**, 294 (2014).
[4] M. K. Verma, Phys. Scr. **94**, 064003 (2019).
[5] M. K. Verma, J. Phys. A: Math. Theor. **55**, 013002 (2022).
[6] A. Maffioli, J. Fluid Mech. **870**, 266 (2019).
[7] A. Maffioli, Phys. Rev. Fluids **2**, 104802 (2017).
[8] B. R. Sutherland, *Internal Gravity Waves* (Cambridge University Press, Cambridge, 2010).
[9] P. Monti, G. Querzoli, A. Cenedese, and S. Piccinini, Phys. Fluids **19**, 085104 (2007).
[10] J. Rotter, H. J. S. Fernando, and E. Kit, Phys. Fluids **19**, 065107 (2007).
[11] M. van Aartrijk, H. J. H. Clercx, and K. B. Winters, Phys. Fluids **20**, 025104 (2008).
[12] F. Karimpour and S. K. Venayagamoorthy, Phys. Fluids **27**, 046603 (2015).
[13] J. J. Riley and M.-P. Lelong, Annu. Rev. Fluid Mech. **32**, 613 (2000).
[14] M. Gregg, E. D'Asaro, J. Riley, and E. Kunze, Annu. Rev. Mar. Sci. **10**, 443 (2018).
[15] C. Caulfield, Annu. Rev. Fluid Mech. **53**, 113 (2021).
[16] M. K. Verma, A. Kumar, and A. Pandey, New J. Phys. **19**, 025012 (2017).
[17] R. Bolgiano Jr., J. Geophys. Res. **64**, 2226 (1959).
[18] D. Rosenberg, A. Pouquet, R. Marino, and P. D. Mininni, Phys. Fluids **27**, 055105 (2015).
[19] E. Lindborg, J. Fluid Mech. **550**, 207 (2006).
[20] D. Buaria, A. Pumir, F. Feraco, R. Marino, A. Pouquet, D. Rosenberg, and L. Primavera, Phys. Rev. Fluids **5**, 064801 (2020).
[21] W. D. Smyth and J. N. Moum, Phys. Fluids **12**, 1343 (2000).
[22] G. Brethouwer, P. Billant, P. Billant, E. Lindborg, and J.-M. Chomaz, J. Fluid Mech. **585**, 343 (2007).
[23] A. M. Obukhov, Dokl. Acad. Nauk SSSR **125**, 1246 (1959).
[24] Y. Kimura and J. R. Herring, J. Fluid Mech. **328**, 253 (1996).
[25] A. Kumar, A. G. Chatterjee, and M. K. Verma, Phys. Rev. E **90**, 023016 (2014).
[26] A. Kumar and M. K. Verma, Phys. Rev. E **91**, 043014 (2015).
[27] J. K. Bhattacharjee, Phys. Lett. A **379**, 696 (2015).
[28] J. K. Bhattacharjee, Philos. Trans. R. Soc. A **380**, 20210075 (2022).
[29] A. Basu and J. K. Bhattacharjee, Phys. Rev. E **100**, 033117 (2019).
[30] R. Agrawal and A. J. Chandy, Intl. J. Heat Fluid Flow **89**, 108778 (2021).
[31] S. Alam, A. Guha, and M. K. Verma, J. Fluid Mech. **875**, 961 (2019).
[32] J. K. Bhattacharjee, Phys. Lett. A **417**, 127682 (2021).
[33] S. Wunsch and A. Kerstein, Phys. Fluids **13**, 702 (2001).
[34] R. Mohapatra, C. Federrath, and P. Sharma, MNRAS **500**, 5072 (2020).
[35] O. M. Phillips, Deep-Sea Res. **19**, 79 (1972).
[36] P. Billant and J.-M. Chomaz, Phys. Fluids **13**, 1645 (2001).
[37] Y.-G. Park, J. A. Whitehead, and A. Gnanadeskian, J. Fluid Mech. **279**, 279 (1994).
[38] P. Augier, P. Billant, M. E. Negretti, and J.-M. Chomaz, Phys. Fluids **26**, 046603 (2014).
[39] J. M. Holford and P. Linden, Dyn. Atmos. Oceans **30**, 173 (1999).
[40] M. L. Waite, Phys. Fluids **23**, 066602 (2011).
[41] P. Augier, P. Billant, and J.-M. Chomaz, J. Fluid Mech. **769**, 403 (2015).
[42] A. Maffioli and P. A. Davidson, J. Fluid Mech. **786**, 210 (2016).
[43] C. J. Howland, J. R. Taylor, and C. P. Caulfield, J. Fluid Mech. **898**, A7 (2020).
[44] S. Remmler and S. Hickel, Theor. Comput. Fluid Dyn. **27**, 319 (2013).
[45] M. L. Waite and P. Bartello, J. Fluid Mech. **517**, 281 (2004).
[46] P. Augier, J.-M. Chomaz, and P. Billant, J. Fluid Mech. **713**, 86 (2012).
[47] J. J. Riley and S. M. deBruynKops, Phys. Fluids **15**, 2047 (2003).
[48] S. M. de Bruyn Kops, J. Fluid Mech. **775**, 436 (2015).
[49] Yu. Cheng, Q. Li, S. Argentini, C. Sayde, and P. Gentine, J. Geophys. Res. Atmos. **125**, e2019JD032191 (2020).
[50] C. Rorai, P. D. Mininni, and A. G. Pouquet, Phys. Rev. E **92**, 013003 (2015).

[51] G. D. Nastrom and K. S. Gage, J. Atmos. Sci. **42**, 950 (1985).
[52] G. D. Nastrom, K. S. Gage, and W. H. Jasperson, Nature (London) **310**, 36 (1984).
[53] J. D. Legaspi and M. L. Waite, J. Fluid Mech. **903**, A12 (2020).
[54] S. Khani and M. Waite, J. Fluid Mech. **754**, 75 (2014).
[55] S. Khani and M. L. Waite, J. Fluid Mech. **773**, 327 (2015).
[56] S. Remmler and S. Hickel, Intl. J. Heat Fluid Flow **35**, 13 (2012).
[57] K. Jadhav and A. J. Chandy, Flow, Turbul. Combust. **106**, 37 (2021).
[58] C. P. Caulfield and R. R. Kerswell, Phys. Fluids **13**, 894 (2001).
[59] M. Rahmani, B. R. Seymour, and G. A. Lawrence, Phys. Fluids **28**, 054107 (2016).
[60] S. Balasubramanian and Q. Zhong, Phys. Fluids **30**, 056601 (2018).
[61] T. Dauxois, T. Peacock, P. Bauer, C. P. Caulfield, C. Cenedese, C. Gorlé, G. Haller, G. N. Ivey, P. F. Linden, E. Meiburg, N. Pinardi, N. M. Vriend, and A. W. Woods, Phys. Rev. Fluids **6**, 020501 (2021).
[62] E. Villermaux, Annu. Rev. Fluid Mech. **51**, 245 (2019).
[63] X. Jiang, A. Lefauve, S. B. Dalziel, and P. Linden, J. Fluid Mech. **947**, A30 (2022).
[64] C. Liu, Y. Gao, S. Tian, and X. Dong, Phys. Fluids **30**, 035103 (2018).
[65] W. Xu, Y. Gao, Y. Deng, J. Liu, and C. Liu, Phys. Fluids **31**, 095102 (2019).
[66] J. J. Riley, J. Fluid Mech. **952**, F1 (2022).
[67] T. R. Osborn, J. Phys. Oceanogr. **10**, 83 (1980).
[68] S. K. Venayagamoorthy and D. D. Stretch, J. Fluid Mech. **644**, 359 (2010).
[69] G. D. Portwood, S. M. de Bruyn Kops, and C. P. Caulfield, Phys. Rev. Lett. **122**, 194504 (2019).
[70] G. Portwood, S. de Bruyn Kops, and C. Caulfield, J. Fluid Mech. **939**, A10 (2022).
[71] J. S. Turner, J. Fluid Mech. **33**, 639 (1968).
[72] H. Kato and O. M. Phillips, J. Fluid Mech. **37**, 643 (1969).
[73] W. R. Peltier and C. P. Caulfield, Annu. Rev. Fluid Mech. **35**, 135 (2003).
[74] R. L. F. Oglethorpe, C. P. Caulfield, and A. W. Woods, J. Fluid Mech. **721**, R3 (2013).
[75] P. Mukherjee and S. Balasubramanian, Phys. Rev. Fluids **5**, 063802 (2020).
[76] P. Mukherjee and S. Balasubramanian, Phys. Rev. Fluids **6**, 013801 (2021).
[77] J. K. Bhattacharjee, A. Kumar, and M. K. Verma, Phys. Scr. **94**, 125008 (2019).
[78] P. D. Ditlevsen, *Turbulence and Shell Models* (Cambridge University Press, Cambridge, 2010).
[79] E. B. Gledzer, Sov. Phys. Dokl. **18**, 216 (1973).
[80] M. Yamada and K. Ohkitani, J. Phys. Soc. Jpn. **56**, 4210 (1987).
[81] K. Ohkitani and M. Yamada, Prog. Theor. Phys. **81**, 329 (1989).
[82] M. Yamada and K. Ohkitani, Phys. Rev. Lett. **60**, 983 (1988).
[83] M. H. Jensen, G. Paladin, and A. Vulpiani, Phys. Rev. A **43**, 798 (1991).
[84] D. Pisarenko, L. Biferale, D. Courvoisier, U. Frisch, and M. Vergassola, Phys. Fluids A: Fluid Dyn. **5**, 2533 (1993).
[85] L. Kadanoff, D. Lohse, J. Wang, and R. Benzi, Phys. Fluids **7**, 617 (1995).
[86] P. Frick, B. Dubrulle, and A. Babiano, Phys. Rev. E **51**, 5582 (1995).
[87] V. S. L'vov, E. Podivilov, A. Pomyalov, I. Procaccia, and D. Vandembroucq, Phys. Rev. E **58**, 1811 (1998).
[88] L. Biferale, Annu. Rev. Fluid Mech. **35**, 441 (2003).
[89] A. Brandenburg, Phys. Rev. Lett. **69**, 605 (1992).
[90] Jiang Mingshun and Liu Shida, Phys. Rev. E **56**, 441 (1997).
[91] S. A. Lozhkin and P. G. Frick, Fluid Dyn. **33**, 842 (1998).
[92] P. Olla, Phys. Rev. E **57**, 2824 (1998).
[93] E. S. C. Ching and W. C. Cheng, Phys. Rev. E **77**, 015303(R) (2008).
[94] E. Suzuki and S. Toh, Phys. Rev. E **51**, 5628 (1995).
[95] P. G. Frik, Magnitnaia Gidrodinamika, 48 (1984).
[96] C. Gloaguen, J. Léorat, A. Pouquet, and R. Grappin, Phys. D: Nonlinear Phenom. **17**, 154 (1985).
[97] D. Biskamp, Phys. Rev. E **50**, 2702 (1994).
[98] V. Carbone, Phys. Rev. E **50**, R671 (1994).
[99] A. Brandenburg, K. Enqvist, and P. Olesen, Phys. Rev. D **54**, 1291 (1996).
[100] P. Frick and D. D. Sokoloff, Phys. Rev. E **57**, 4155 (1998).
[101] R. Stepanov and F. Plunian, J. Turbul. **7**, N39 (2006).
[102] P. A. Davidson, *Turbulence: An Introduction for Scientists and Engineers* (Oxford University Press, Oxford, 2004).
[103] M. K. Verma, *Energy transfers in Fluid Flows: Multiscale and Spectral Perspectives* (Cambridge University Press, Cambridge, 2019).
[104] M. K. Verma, S. Alam, and S. Chatterjee, Phys. Plasmas **27**, 052301 (2020).
[105] S. S. Ray, D. Mitra, and R. Pandit, New J. Phys. **10**, 033003 (2008).
[106] D. Biskamp, *Magnetohydrodynamic Turbulence* (Cambridge University Press, Cambridge, 2003).
[107] K. P. Zybin, V. A. Sirota, and A. S. Ilyin, Phys. Rev. E **82**, 056324 (2010).
[108] K. P. Zybin and V. A. Sirota, Phys. Rev. Lett. **104**, 154501 (2010).
[109] R. Benzi, L. Biferale, R. Fisher, D. Q. Lamb, and F. Toschi, J. Fluid Mech. **653**, 221 (2010).
[110] W. van de Water and J. A. Herweijer, Phys. Scr. **1996**, 136 (1996).
[111] R. Mohapatra, C. Federrath, and P. Sharma, MNRAS **493**, 5838 (2020).
[112] R. Stepanov and F. Plunian, Astrophys. J. **680**, 809 (2008).
[113] O. D. Gürcan and R. Grappin, Phys. Rev. E **84**, 066308 (2011).
[114] V. Carbone and P. Veltri, Geophys. Astrophys. Fluid Dyn **52**, 153 (1990).